JOURNAL OF APPLIED ELECTROCHEMISTRY **28** (1998) 1051–1059

Behavior of lithiated graphite electrodes comprising silica based binder

D. AURBACH, M. D. LEVI

Department of Chemistry, Bar-Ilan University, Ramat-Gan 52900, Israel

O. LEV, J. GUN, L. RABINOVICH

Laboratory of Environmental Chemistry, Division of Environmental Sciences, Fredy and Nadine Hermann School of Applied Science, The Hebrew University of Jerusalem, Jerusalem 91904, Israel

Received 24 September 1997; revised 21 April 1998

Graphite electrodes comprising silica binder were tested in ethylene carbonate–dimethyl carbonate (EC–DMC), propylene carbonate and tetrahydrofuran solutions. The electrochemical behavior of these electrodes was analyzed using chronopotentiometry, slow-scan rate cyclic voltammetry (SSCV), impedance spectroscopy and potentiostatic intermittent titration technique (PITT). The electrode morphology and integrity were studied by scanning electron microscopy (SEM). Using silica binder, graphite particles are usually embedded in the current collector in an unoriented form. Thus, the electroanalytical study of these electrodes and the comparison of their response with that of highly oriented PVDF based graphite electrodes, provided insight into the effect of particle orientation on the general electrochemical behavior of lithiated graphite anodes. In general, the higher the particle orientation and compact packing in the electrodes' active mass, the better the performance of the Li–graphite electrodes, as the surface films developed are better passivating and the interparticle electronic contact is also better. The silica binder may have advantages over other binders such as PVDF in its ability to better retain the electrode integrity upon cycling. However, the practical use of such electrodes requires further optimization, especially in connection with particle orientation and compact packing.

Keywords: *Carbon-Ceramic electrodes*, *Li ion batteries*, *intercalation*, *Li salt solutions*, *EIS*, *sol-gel*, *Ormosil*

1. Introduction

Recent development and commercialization of Li-ion batteries has focused attention on basic studies of the insertion of lithium into carbonaceous materials which serve as anodes in these battery systems. These studies included performance analysis (electrochemical measurements) [1–5], structural analysis (XRD) [6–9], solid state Li-ion diffusion [10–13], and the surface chemistry developed on the carbons in solutions [14–19].

We have extensively studied stabilization and failure mechanisms of Li–graphite electrodes [20] and explored their electroanalytical behavior using a variety of techniques, including slow-scan rate cyclic voltammetry (SSCV), impedance spectroscopy (EIS), potentiostatic intermittent titration (PITT) and chronopotentiometry in conjunction with surface sensitive FTIR spectroscopy, photoelectron spectroscopy (XPS), X-ray diffractometry (XRD) and scanning electron microscopy (SEM) [21–25].

Synthetic graphite platelets are usually thin flakes which slide easily over each other. Using a PVDF binder, highly oriented electrodes are formed in which the graphite particle's basal planes are parallel to the current collector.

The electrochemical intercalation into these electrodes includes several processes which occur in series: Li diffusion in solution phase, Li^+-ion transfer across solution/surface film interface and its subsequent migration through the surface films, charge transfer by electrons (which compensates the charge of the intercalating Li ions), solid state diffusion of Li in the graphite bulk, and, finally, accumulation of Li in the bulk and phase transition between the various intercalation stages [21–25]. The degree of separation amongst these processes, as probed by the various techniques, depends on the thickness and orientation of the active mass and the characteristic time window of the experiment (e.g. scan rate for CV, frequency range in EIS and time domain used for PITT).

At certain potential domains (and intercalation levels) in which two phases coexist, the intercalation differential capacity has maxima and the Li diffusion coefficient has minima. Consequently, the SSCV is characterized by three distinctive peaks for both intercalation and deintercalation processes, while D vs. E (or X) is a non-monotonic function which has minima at the CV peak potentials. It was

0021-891X

clear from previous work that when a PVDF binder is used, the electrodes are sufficiently porous, allowing the solution to percolate and reach the entire active mass of the electrode. On the other hand, it seems that PVDF is highly flexible and does not interfere with any of the graphite particle processes where volume expansion is involved. Depending on the electrolyte solution used, we analyzed several destructive processes of Li–graphite anodes in which coinsertion of solvent molecules with Li ions and/or gas formation due to surface reduction of the solvent molecules led to exfoliation of graphite particles and electrical disconnection of the active mass from the current collector. It is possible that harder binding materials may contribute to the stability of the graphite particles in the electrodes and prevent easy exfoliation. We have recently introduced silicate-graphite composite electrodes [26] and demonstrated lithium intercalation in these matrices [27].

In the present work we studied the electrochemical behavior of graphite electrodes in which a silica-based binder was used. Such a binder should be harder than PVDF and may thus provide more stability of the active mass.

Three solutions were used. In order to probe the behavior of stable electrodes on which stable and highly passivating surface films are formed, an ethylenecarbonate–dimethylcarbonate (EC–DMC) mixture with $LiAsF_6$ 1 M was used. $LiAsF_6$ solutions in THF and PC were also tested in order to see whether the use of silica-based binder improves the electrode stability and reversibility in these solutions (which are usually poor when a PVDF binder is used). SEM, SSCV, PITT, EIS and chronopotentiometry were used for the electrochemical analysis of the electrodes.

2. Experimental details

Graphite particles from Lonza (KS-6), solvents from Merck (EC, DMC) and Tomiyama (EC, DMC, THF and PC), all highly pure, Li battery grade, $LiAsF_6$ from Lithco and lithium foils from Foote Minerals were used. The graphite electrodes were prepared as follows: 1 ml of the methyl-tri-methoxysilane (from ABCR Inc, Karlsruhe), 6 ml of methanol (from Frutarom Lab. Chem., Haifa), 0.05 ml of HCl catalyst (11 M) and 0.2 ml of distilled water were mixed together for 2 min. 1 g of synthetic graphite (KS-6 Lonza) was then added and the mixture was sonicated for 2 min. A copper foil was cut into the appropriate size ($1.2 \times 1.2\,cm^2$) and covered with the as-prepared sonicated electrode slurry. The electrodes were then dried at ambient temperature (25 °C) for 48 h. Typically, the electrodes were about 8 mg in weight and 25–30 μm in thickness (15–25% by weight of the binder). Hence, the electrode mass comprised graphite particles bound with a matrix based on methyl-silicate.

For comparison, ultrathin, thin and thick graphite electrodes comprising Lonza KS-6 particles and PVDF binder (<0.5, 10 and 150 μm, respectively) prepared as already described [21–24], were also tested. Standard three electrode cells with Li foils, counter and reference electrodes were used. SSCV, PITT and EIS were performed using the Schlumberger 1286 EI and 1255 FRA driven by Corrware and Zplot software from Scribner Ass. (PC 586). Prolonged cycling was performed using the Maccor model 2000 battery tester. The SEM measurements, the relevant transfer technique and the instrumentation were described earlier [15, 16, 20, 25]. All the solution preparations and cell assemblies were carried out under high purity argon in a VAC glove box. All the electrochemical measurements were performed outside the glove box in thermostatted (25 °C), hermetically sealed aluminum vessels.

3. Results and discussion

Graphite electrodes comprising silica binder were cycled in dry (20 ppm of H_2O) EC–DMC, THF and PC solutions containing $LiAsF_6$. A standard galvanostatic experiment in which the electrodes were cycled at a $C/9$ h rate was applied. The results were compared with parallel experiments with similar electrodes comprising a PVDF binder. As expected, the reversibility, stability and capacity of all the electrodes in EC–DMC solutions were very high and about 95% of the active mass was involved in the reversible cycling. Careful linear sweep voltammetric studies of these electrodes in the potential range between OCV ($\approx$3 V vs Li/Li^+) and the foot of the intercalation potential (0.25 V vs Li/Li^+) indicated that the silica binder was not electroactive.

It was impossible to obtain reversible intercalation of lithium in PC solutions. Hence, the use of the silica binder made no difference compared with PVDF. The similarity in the behavior of the two types of electrodes in the above solutions is expected. The electrode stabilization by the surface films formed in EC–DMC is very efficient, while in PC it is very poor and, hence, the effect of the binder used is not too important in these extreme cases.

A much better method of examining the effect of the binder may be by the use of THF solutions. As already demonstrated [20], in dry, uncontaminated THF solutions, lithium cannot be intercalated reversibly into graphite. However, slight changes in the THF solution composition, such as increasing the amount of water contamination or the addition of low concentration of alkyl carbonate cosolvent, completely changed the behavior of lithiated graphite electrodes to reversible.

Figure 1 presents a typical chronopotentiogram obtained from a cycling experiment of the silica-based electrode in dry (20 ppm H_2O) THF solution. This figure also shows the capacity vs cycle number (X of Li in Li_xC_6) during the first few cycles. For comparison, a typical chronopotentiogram obtained from a PVDF based electrode in a similar experiment

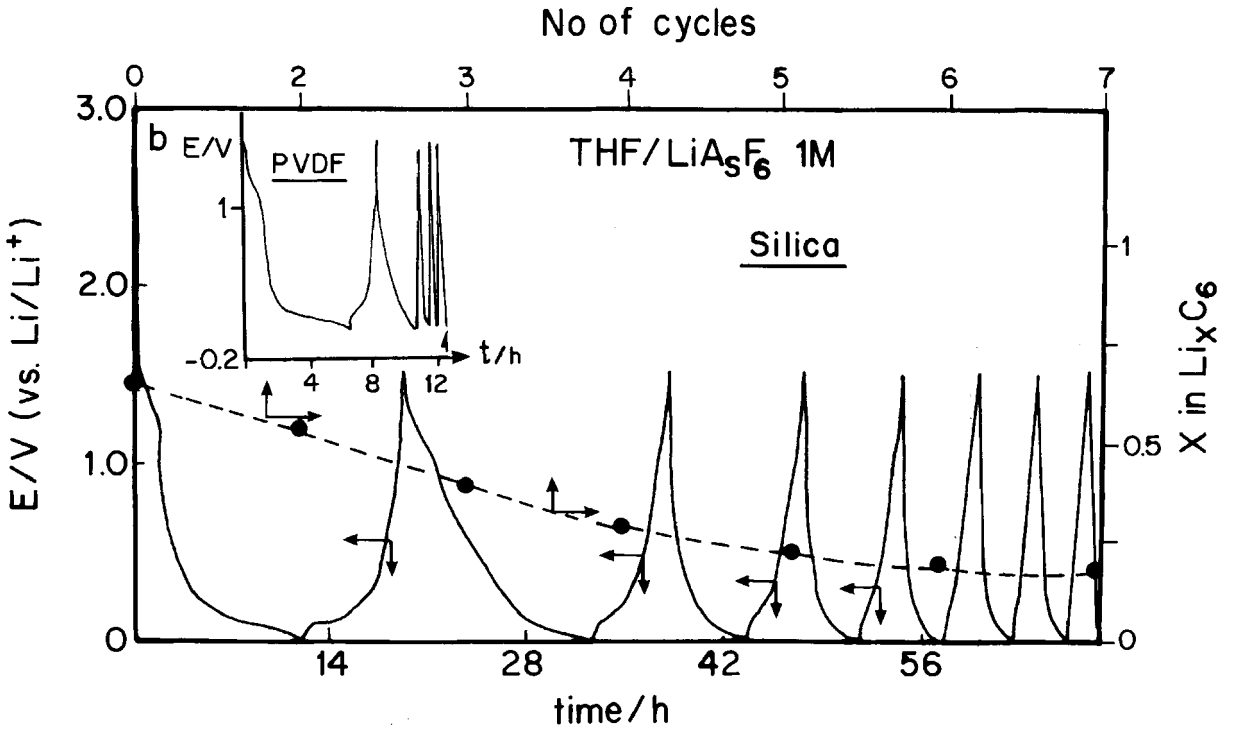

Fig. 1. Chronopotentiometry (E vs t, at a constant current 0.4 mA for a graphite–silica electrode (9.8 mg of graphite KS-6). The decay of capacity (X of Li^+ vs Li_xC_6) as a function of cycle number is also shown. For comparison, a chronopotentiometric curve for the graphite electrode with a PVDF binder is shown.

is also shown. This figure seems to show that the behavior of the silica-based electrode is slightly better than that of the PVDF based one, in terms of capacity, stability and reversibility.

Figure 2 presents SEM micrographs obtained from graphite electrodes. Figure 2(a) shows the pristine electrodes, while Fig 2(b) and (c) show electrodes cycled once (intercalation–deintercalation cycle) in $LiAsF_6$ 1 M solutions of EC–DMC and PC, respectively.

These morphological studies lead to the following conclusions:

(i) The graphite platelets in the electrodes comprising the silica binder are highly disoriented, in contrast to the standard electrodes prepared with the PVDF binder [20–24]. Hence, the study of these electrodes provides a good opportunity to better understand the influence of the particle orientation on the electroanalytical response of lithiated graphite electrodes.

(ii) As expected, after even one cycle in the solutions, the active mass is covered with visible surface films.

(iii) As already shown [20], graphite electrodes comprising PVDF, when polarized to low potentials in PC solutions, follow pronounced morphological changes. When the binder is silica, the electrodes treated in PC remained integrated with no pronounced change in the particle orientation and morphology (except for the visible formation of surface species, Fig. 2). Hence, the failure of these electrodes to intercalate reversibly with lithium in PC may be attributed mostly to processes on the particle surface which insulate them from the current collector. When passivation by the surface species formed on the graphite particles is poor (as is the case for PC solutions), their massive precipitation may interfere badly with the electrical contact amongst the graphite particles [20].

Figure 3 compares a typical SSCV of the silica-based electrode with that of a practical PVDF based electrode (150 μm thick) and that of an ultrathin electrode (submicronic thickness, PVDF). The solution chosen for these studies was EC–DMC 1 M $LiAsF_6$ in which the Li–C intercalation is highly reversible, as discussed above. The curves of Fig. 3, as well as the results of all the other electroanalytical studies described below, were obtained after stable surface films were formed on the electrode surface, and thus reflect steady state behavior. For comparison, the currents for thick electrodes were normalized with those for the ultrathin one by multiplying them by the mass ratio $m_{\text{ultrathin}}/m_{\text{thick}}$. Such a presentation enabled the display of the three CVs on the same scale and a comparison of their shape. These voltammetric curves are typical of the Li–graphite intercalation process and show three distinctive reversible red–ox processes which relate to the phase transition between the various intercalation stages. (Diluted Stage I $\leftrightarrow$ Stage IV, Stage III $\leftrightarrow$ Stage II, Stage II $\leftrightarrow$ Stage I.) As already discussed [21, 25], as the peaks are sharper and better resolved, they reflect the accumulation of Li in the bulk graphite and the phase transition, with less interference by other relaxation processes (interfacial processes, charge transfer, solid

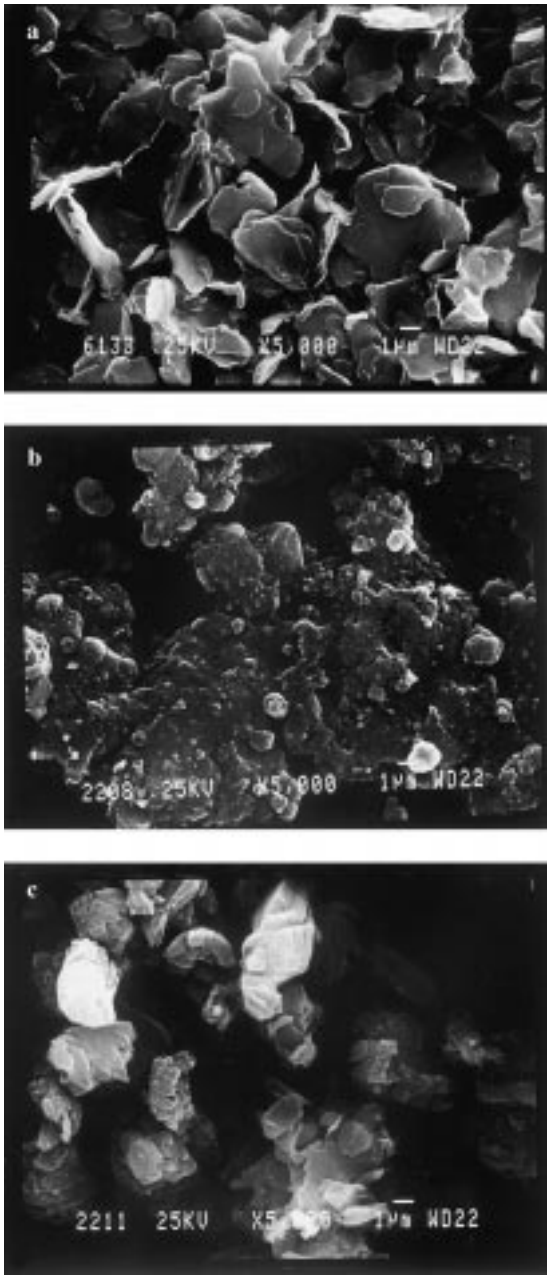

Fig. 2. SEM micrographs obtained from (a) pristine silica–graphite before the electrochemical treatment; (b) after cycling in 1 M $LiAsF_6$/EC + DMC and (c) in 1 M $LiAsF_6$/PC solutions.

state diffusion, etc.). The curves in Fig. 3 differ from each other. The CV peaks from the ultrathin electrode are the sharpest and are well resolved. The CV peaks of the thicker electrodes are much broader. It is significant that the CV peaks of the silica-based electrode are broader than those of the PVDF based electrode.

These differences in the CV curves reflect the differences in the electrode structure. As the electrode is less compactly packed, and its particles are less oriented, the separation of the various processes occurring in series along the intercalation path by electroanalytical tools such as CV is more difficult. Hence, despite the slow-scan rate applied, the relatively broad peaks of the CV obtained from the silica-based electrode should be attributed to the low degree of orientation of the graphite particles.

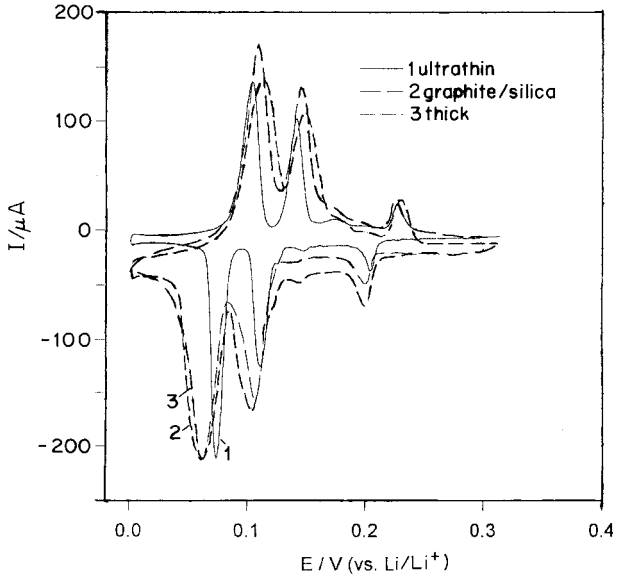

Fig. 3. Cyclic voltammograms for the graphite/silica electrode and ultrathin and thick graphite/PVDF electrodes at $\upsilon = 4\,\mu V\,s^{-1}$. For comparison, the current was normalized with respect to their relative masses (see text).

Figure 4 compares the effect of the scan rate on the shape of cyclic voltammograms obtained with a silica-based electrode and further demonstrates the effect of the electrode structure on its electroanalytical response. Increasing the scan rate drives the electrochemical processes reflected by the CV toward diffusion and charge transfer control. In the case of the ultrathin electrodes, the CV retains its peak-shaped structure even when the scan rate increases to $50\ \mu V\,s^{-1}$, whereas for the silica-based electrodes. the CV becomes featureless at $\upsilon > 15$–$20\,\mu V\,s^{-1}$. This means that this electrode is relatively slow, and even at quite a low scan rate (15–$20\,\mu V\,s^{-1}$) its electrochemical behavior is diffusion controlled.

A comparative study of the graphite electrodes by impedance spectroscopy may better clarify what the key factors are that determine their electroanalytical behavior. In the present study, we compared the impedance spectra measured from the silica-based electrodes with those obtained from ultrathin (submicron), thin (10 μm) and thick (100–150 μm) PVDF based electrodes.

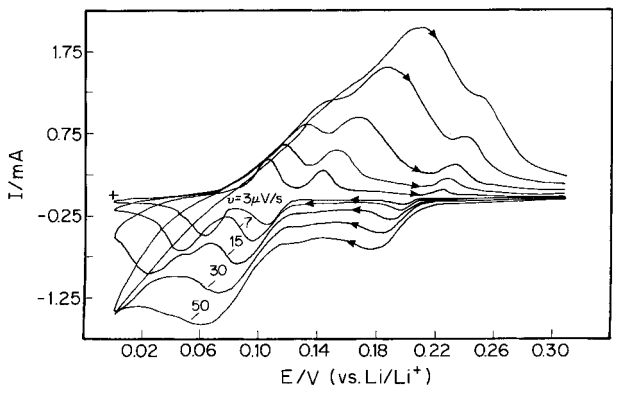

Fig. 4. Cyclic voltammograms for the graphite/silica electrodes (5.2 mg of KS-6) at different potential scan rates υ ($\mu V\ s^{-1}$) shown in the figure.

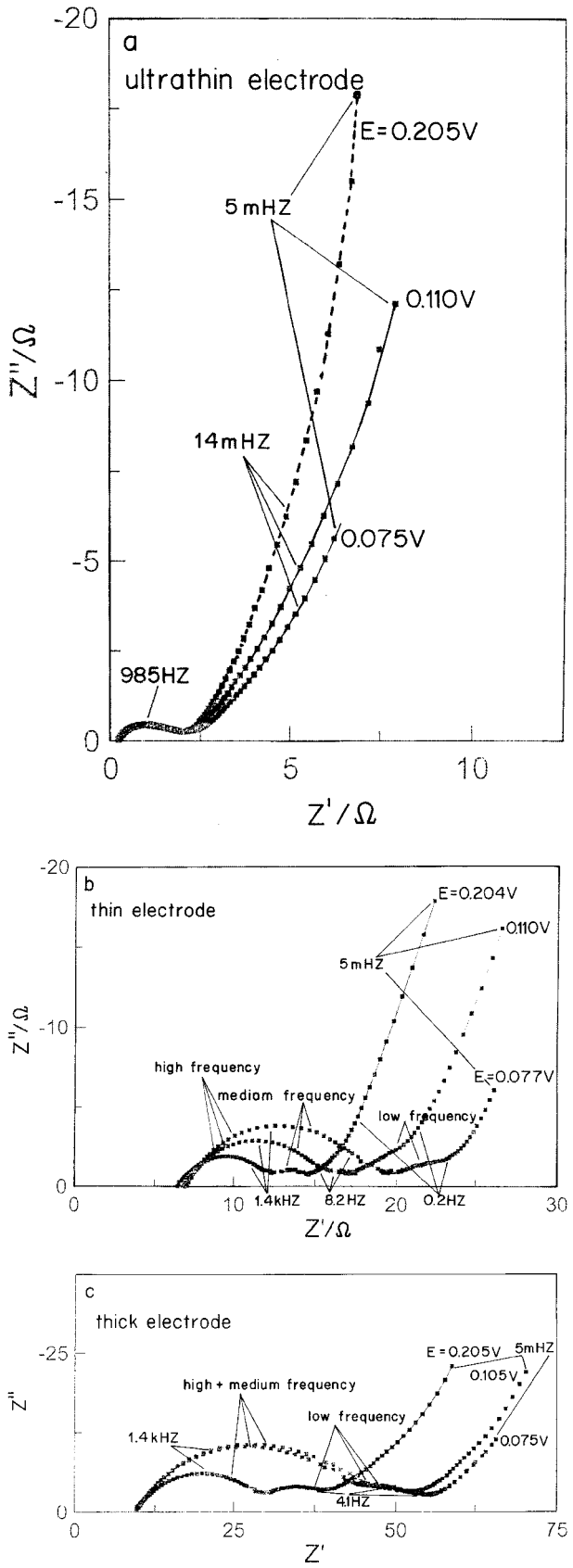

Fig. 5. Nyquist plots measured from (a) an ultrathin, (b) thin and (c) thick graphite/PVDF electrode. The range of frequencies used was from 100 kHz to 5 mHz. The Z', Z'' values for the thin and ultrathin electrodes were normalized with respect to the thick electrode by multiplying them by the mass ratio (see text).

Figure 5 presents Nyquist plots obtained from the ultrathin, thin and thick PVDF based electrodes (Fig. 5(a)–(c), respectively) at the three potentials in which the cyclic voltammograms of these electrodes show peaks (Fig. 3). The spectra of the thin electrodes were normalized compared with the thick ones by multiplying their Z'' and Z' values by their mass ratio (m_{thick}/m_{thin} or $m_{thick}/m_{ultrathin}$). As already discussed [23], this normalization procedure is based on the fact that all the various processes taking place, including Li^+ migration through surface films, solid-state diffusion and Li accumulation, occur through a cross-sectional area perpendicular to the basal planes of the graphite particles, which is in fact the envelope of the facets perpendicular to the wide dimension of the particles (see Fig. 2). The total cross-sectional area of the electrodes for all the electrochemical processes, and thus for their impedance, is directly proportional to the number of graphite particles per electrode and, thus, to the total active mass. Consequently, the electrode impedance is inversely proportional to this cross-sectional area, and to the active mass.

All the impedance spectra appearing in Fig. 5 have common features: a big semicircle related to the high frequency, another small semicircle related to the medium frequencies. At low frequencies, Z'' vs Z' is a straight line attributable to a Warburg type element, and this line becomes steeper as the frequency is lower. At very low frequencies (mHz region) Z'' vs Z' becomes a nearly vertical line, which reflects capacitive behavior.

Figure 5(b) is typical of thin electrode behavior and shows the evolution of a third (low-frequency) semicircle which becomes distinctly expressed only at a relatively high intercalation level (i.e. at a low potential). This semicircle is formed on account of the length of the frequency range of the Warburg domain. As shown in Fig. 5(c), for thicker electrodes, the low-frequency semicircle is observed even at relatively low values of X (i.e. at high potentials). For the ultrathin electrode only one single high-frequency semicircle appears on the corresponding Nyquist plots.

The high frequency (big) semicircle in the spectra of Fig. 5 relates to Li^+-ion migration through the surface films which cover the graphite and, hence, the diameter of this semicircle is the surface film resistance to Li-ion transfer (which is coupled with the film capacitance) [23]. The medium frequency semicircle is attributed to an interfacial charge transfer resistance due to electronic and/or interfacial Li-ion transfer. As X increases, this semicircle tends to overlap with the bigger (high-frequency) one which considerably complicates the analysis. The low-frequency semicircle may be related to electron transfer across the boundaries between the graphite particles covered with surface films. This resistance should depend on the electric contact amongst the graphite particles. The Warburg type element appearing at the low frequencies reflects the solid state diffusion of lithium into the bulk graphite. Finally, the steep Z'' vs Z' plot at the very low frequencies reflects a capacitive behavior of the electrodes. The effect of the

electrode structure on its impedance spectra may be understood as follows: For the ultrathin electrode whose particles are highly oriented and compactly packed, the big semicircle is the smallest, the medium and the low frequency semicircles do not appear, and the very low-frequency behavior is almost purely capacitive. The thicker the electrode the larger the high frequency semicircle, the medium frequency semicircle is more developed and the very low-frequency behavior is not purely capacitive. It is assumed that as the graphite particles are less oriented, there are many voids within the electrode active mass. This leads to a poor electrical contact amongst the particles, and to the formation of surface films which are less passivating and more resistive. Consequently, the resistance for Li^+-ion migration and for the interfacial charge transfer due to electron transfer across the particle boundaries is higher. There is a possible continuous reduction of solution species in the voids (due to the poor passivation by the surface films formed on the less oriented electrodes). Thereby, the thick electrodes cannot reach pure capacitive behavior, even at prolonged relaxation time, because the accumulation of Li in the bulk is always accompanied by parasitic reduction of solution species.

Figure 6 shows typical Nyquist plots obtained with a silica-based electrode at different potentials during the Li intercalation process. The electrode was measured after being cycled several times in the solution (EC–DMC 1 M $LiAsF_6$), and thus the surface films are fully developed, although not necessarily fully passivating. Figure 7 presents typical Nyquist plots obtained with the same electrode at different potentials during deintercalation of lithium from these electrodes. The plots of Figs 6 and 7 differ from those obtained from the more oriented PVDF based electrodes discussed above. They reflect more resistive electrodes, especially in the elements related to the surface films and the electron transfer (high-medium to low frequencies). This electrode resistance increases as the potential is lower. In addition, the low-frequency domain does not reflect a capacitive behavior.

It is clear that the spectra of Figs 6 and 7 reflect a typical behavior of unoriented graphite electrodes whose active mass is porous, containing many voids. This initial structure prevents the formation of compact surface films, and, therefore, the intercalation process may be accompanied by continuous reduction of solution species even at prolonged relaxation times (as discussed above for thick PVDF based electrodes). A part of the plots in Figs 6(b) and (c)

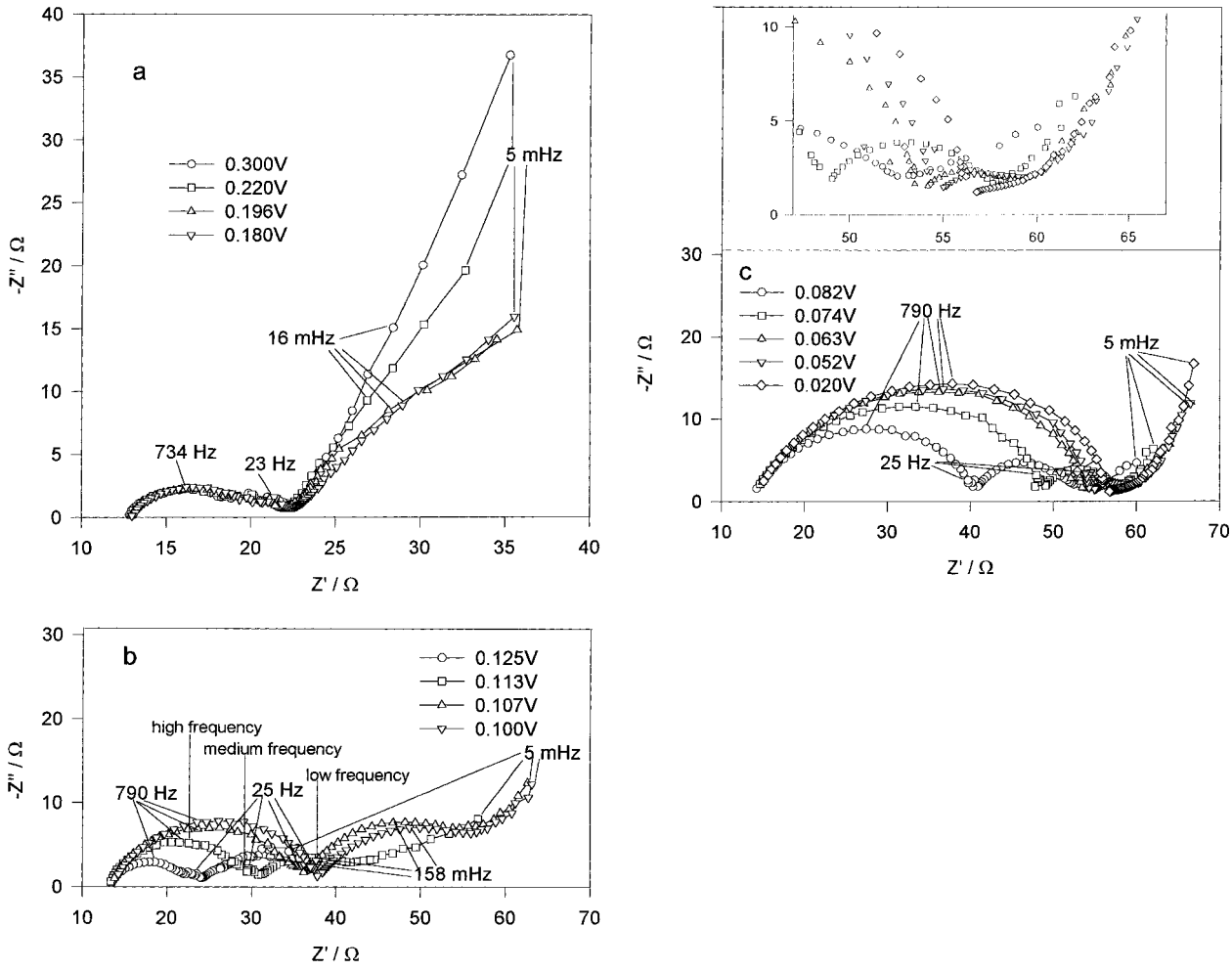

Fig. 6. Nyquist plots measured from a graphite/silica electrode at the beginning ((a) diluted I/IV stages), in the middle ((b) III/II stages) and at the end of the intercalation ((c) II/I stages). The range of frequencies used was the same as indicated in Fig. 5. In Fig. 6(c), a part of the low-frequency domain is presented on an enlarged scale.

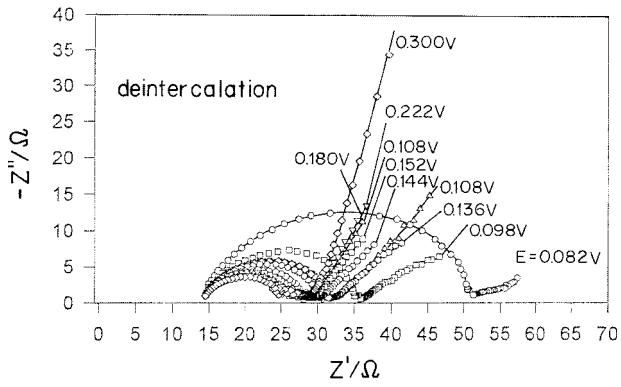

Fig. 7. Nyquist plots measured from a graphite/silica electrode during the deintercalation process (in reverse to the intercalation stages and the relevant Nyquist plots of Fig. 6).

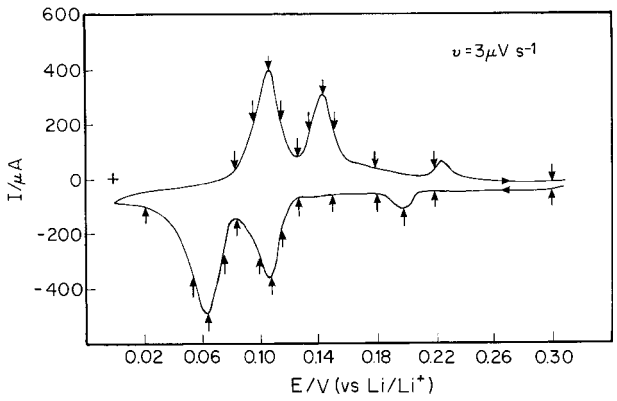

Fig. 8. Slow-scan rate ($\upsilon = 3\ \mu V\ s^{-1}$) cyclic voltammogram of a graphite/silica electrode. The arrows show the potentials at which Nyquist plots were measured. 31 PITT measurements were performed during intercalation with typical potential steps from 1 to 3 mV around the voltammetric peaks and of 50 mV along the flat portions of the CV.

(e.g. for 0.113, 0.107 and 0.074 V vs Li/Li^+) are typical of distorted spectra measured when the electrode cannot reach complete equilibrium. This may be understood as being the result of a small background Faradaic current due to continuous reduction of solution species.

In contrast, the spectra measured at the same potentials during deintercalation (Fig. 7) are typical of graphite electrodes at equilibrium conditions. Hence, it is possible that during deintercalation the parasitic reduction of solution species is suppressed. The increase in the electrode impedance measured for these systems as the potential is lowered (Fig. 6(b) and (c)) is not yet understood. However, it should be noted that this change is reversible (Fig. 7). It is possible that this behavior relates to the increasing concentration of Li ions in the graphite phase in the vicinity of the surface films, as the potential is lower, which increases the surface film resistance.

Comparison between the Nyquist plots for the silica–graphite electrode (Fig. 6(a)–(c)) and that for the ultrathin, thin and thick graphite electrodes based on a PVDF binder (Fig. 5(a)–(c)) helps in understanding the reason for the broadening of the peaks in the SSCV for the former electrode (Fig. 3). This feature of the voltammetric response is mainly connected with the overlap between the Li-ion accumulation step (the low-frequency pure capacitive element of the electrodes' impedance) and solid-state diffusion, and/or the charge transfer across the particles' boundaries.

Figure 8 presents an SSCV of the silica-based electrodes with arrows which mark the potentials at which potentiostatic intermittent titration was applied. Plotting $It^{1/2}$ vs $\log t$ for each of these potential steps provides the family of curves presented in Fig. 9. Each of these curves has a minimum, which is a plateau (const. $It^{1/2}$ vs t), at a certain time. This plateau corresponds to the Cottrell region, and the diffusion coefficient is calculated from this plot in this region from the following equations: [22, 24, 28, 29]

$D = l^2/\tau$, $\tau = (Q_t \Delta X / It^{1/2})^2$ at $t \ll \tau$. τ is the characteristic diffusion time (dependant on E and X), $Q_t \cdot \Delta X$, the intercalation charge related to a specific potential step (Q_t is the total electrode capacity), I, the current measured (vs t), and l, the characteristic diffusion length which in this case is 3 μm, i.e. half the average particle size [21–24].

Figure 10 presents plots of $\log D$ vs X (the mole fraction of Li in Li_xC_6) calculated from PITT for silica-based electrodes and for an ultrathin PVDF based electrode (EC–DMC 1 M $LiAsF_6$). Both plots reflect the non-monotonous behavior of D vs X, E. The three minima observed fall at the X and E values of the peak current in the slow SSCV (Figs 3 and 8).

Figure 11 shows the intercalation capacity (C_{int}/F) calculated from CV and PITT experiments with a silica-based electrode as a function of X. The relevant formulae are: [30]

$$C_{int} = dQ/dE = I/\upsilon \quad (CV)$$

I and υ are the current and the potential scan rate.

$$C_{int} = \Delta Q/\Delta E \quad (PITT)$$

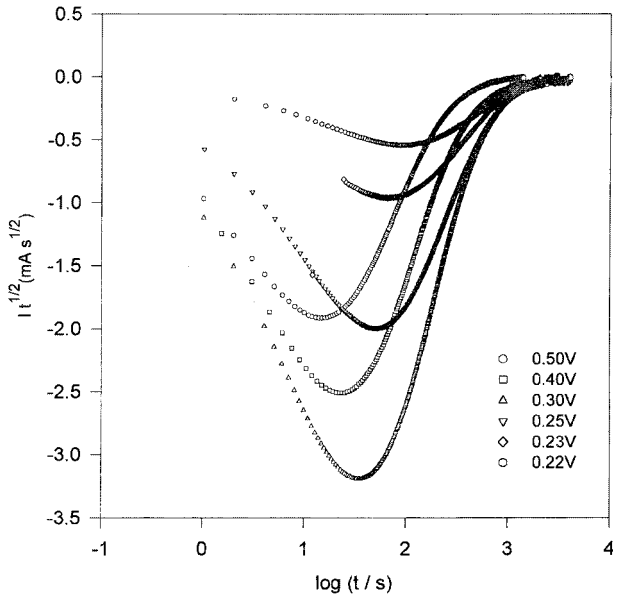

Fig. 9. $It^{1/2}$ vs $\log t$ plots for small potential steps applied around the potentials of the transition between diluted phase I and phase IV.

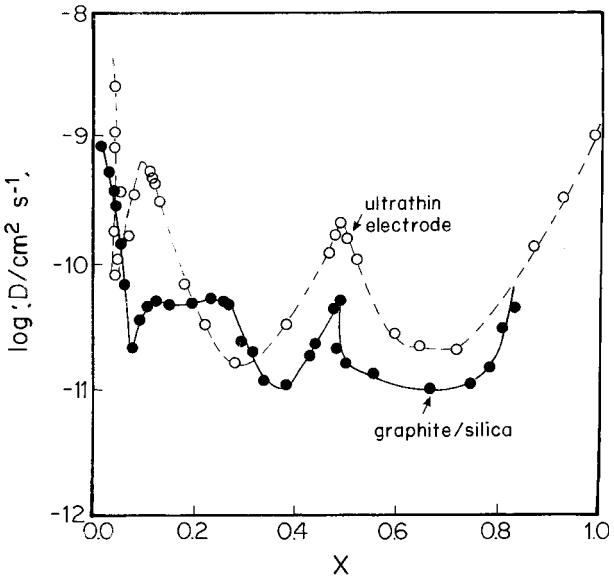

Fig. 10. Log D vs X (x of Li in Li_xC_6) plots calculated from the PITT data for the graphite/silica and ultrathin graphite/PVDF electrodes.

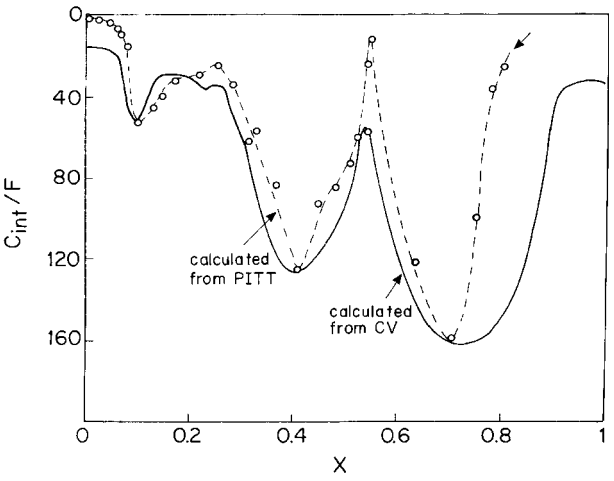

Fig. 11. Comparison between the differential intercalation capacity of the graphite/silica electrode calculated from PITT and CV data.

ΔE is the potential step and ΔQ, the accumulated charge.

The results obtained from the two methods converge and show a non-monotonic behavior in which three maxima in the intercalation capacity appear at the same potentials of the peak currents in the SSCV and the minima in D (Fig. 10). The peaks of C_{int} calculated from PITT are narrower than those obtained from the CV. This means that the former experiment was performed under conditions closer to equilibrium than the latter. The appearance of narrow peaks is typical of an intercalation process in which highly attractive interactions exist amongst the intercalation sites, and a phase transition between two intercalation stages or compounds takes place [23]. In spite of the difference in structure, and hence in the impedance behavior of the silica-based electrode compared with the highly oriented PVDF based ultrathin electrode, Fig. 10 shows an appreciable similarity in the behavior of D vs E, X for the two electrodes. This can be explained as follows. Both electrodes comprise the same particles which are graphite flakes of a submicronic thickness and an average basal plane dimensions of about 6 μm. Using PITT and calculations based on the Cottrell region (after very short relaxation times), the solid-state diffusion process of lithium in the bulk is in focus, with relatively little interference by the other processes (such as Li^+-ion migration through the surface films, charge transfer, etc.). Since in all types of graphite electrodes discussed above, the solution is in contact with all the active mass, the solid-state diffusion is a process which occurs simultaneously in all the graphite particles, and is thereby determined only by the dimension of the single particle. It is thus expected that D calculated from PITT for the solid-state diffusion which reflects simultaneous solid-state processes in the graphite particles should not be strongly affected by the morphology of the electrodes and their particle orientation.

5. Conclusion

Graphite electrodes comprising silica as the binder were examined. The cycling behavior of the silica-based electrodes in EC–DMC base solutions is as good as that of the commonly used PVDF based electrodes. Preliminary studies indicate that the silica-based binder may have some advantage over PVDF in the ability to better retain the electrode's integrity during prolonged cycling. In principle, silica-based electrodes show the typical electroanalytical response of PVDF based graphite electrodes. However, in the absence of special compression during their preparation, the active mass of the silica bound graphite electrodes is highly unoriented. Disorientation of the graphite flakes leads to a porous structure, limited electrical contact amongst the graphite particles, and to an overall situation in which the surface films, which usually cover the graphite particles in Li battery electrolyte solutions at low potentials, are not fully passivating. These are clearly reflected by the electroanalytical response of these electrodes (e.g. high impedance, high steady state background current, and limited peak resolution in SSCV).

These electroanalytical studies prove that the practical use of such a binder depends on the possibility of preparing electrodes of oriented and compactly packed particles.

Acknowledgement

This work was partially supported by the Israeli Ministry of Science.

References

[1] J. R. Dahn, A. K. Sleigh, H. Shi, B. M. Way, W. J. Weydanz, J. N. Reimers, Q. Zhong and U. von Sacken, *in*

'Lithium Batteries, New Materials, Developments and Perspectives' (edited by G. Pistioa), ch. 1, Elsevier, Amsterdam, (1994) pp. 1–47 and references therein.
[2] K. Sawai, Y. Iwakoshi and T. Ohzuku, *Solid State Ionics* **69** (1994) 273.
[3] O. Chusid (Youngman), Y. Ein-Eli, D. Aurbach, M. Babai and Y. Carmeli, *J. Power Sources* **43–44** (1993) 47.
[4] T. Zheng, Y. Liu, E. W. Fuller, S. Tseng, U. von Sacken and J. R. Dahn, *J. Electrochem. Soc.* **142** (1995) 2581.
[5] K. Tatsumi, N. Iwashita, H. Sakaebe, H. Shioyama, S. Higuchi, A. Mabuchi and H. Fujimoto, *J. Electrochem. Soc.* **142** (1995) 716.
[6] J. R. Dahn, *Phys. Rev. B* **441** (1991) 9170.
[7] N. Takami, A. Satoh, M. Hara and T. Ohsaki, *J. Electrochem. Soc.* **142** (1995) 371.
[8] T. Ohzuku, Y. Iwakoshi and K. Sawai, *J. Electrochem. Soc.* **140** (1993) 2490.
[9] D. Aurbach and Y. Ein-Eli, *J. Electrochem. Soc.* **142** (1994) 1746.
[10] D. Guyomard and J. M. Tarascon, *J. Electrochem. Soc.* **139** (1992) 937.
[11] M. Morita, N. Nishimura and Y. Matsuda, *Electrochim. Acta* **38** (1993) 1721.
[12] T. Uchida, Y. Morikawa, H. Ikuta and M. Wakihara, *J. Electrochem. Soc.* **143** (1996) 2606.
[13] K. Zaghib, K. Tatsumi, H. Abe, T. Ohsaki, Y. Sawada and S. Higuchi, *in* 'Rechargeable Lithium and Lithium-Ion Batteries' (edited by) S. Megahed, B. M. Barnett and L. Xie), Battery Division, The Electrochemical Society, Inc, Pennington, NJ (1995), p. 121.
[14] Y. Matsumura, S. Wang and J. Mondori, *J. Electrochem. Soc.* **142** (1995) 2914.
[15] D. Aurbach, Y. Ein-Eli, O. Chusid (Youngman), Y. Carmeli, M. Babai and H. Yamin, *J. Electrochem. Soc.* **141** (1994) 603.
[16] D. Aurbach, Y. Ein-Eli, B. Markovsky and A. Zaban, *J. Electrochem. Soc.* **142** (1995) 2882.
[17] D. Aurbach, B. Markovsky, A. Schechter, Y. Ein-Eli and H. Cohen, J. *Electrochem. Soc.* **143** (1996) 3809.
[18] D. Aurbach, A. Zaban, Y. Ein-Eli, I. Weissman, O. Chusid, B. Markovsky. M. D. Levi, E. A. Levi, A. Schechter and E. Granot, *J. Power Sources* **68** (1997) 91.
[19] D. Aurbach, A. Schechter, B. Markovsky, Y. Ein-Eli and V. Koch, *J. Electrochem. Soc.* **143** (1996) L273.
[20] D. Aurbach, M. D. Levi, E. A. Levi and A. Schechter, *J. Phys. Chem. B* **101** (1997) 2195.
[21] M. D. Levi and D. Aurbach, *J. Electroanal. Chem.* **421** (1997) 79.
[22] M. D. Levi, E. A. Levi and D. Aurbach, *Electroanal. Chem.* **421** (1997) 89.
[23] M. D. Levi and D. Aurbach, *J. Phys. Chem. B* (1997) **101**, 4360.
[24] M. D. Levi and D. Aurbach, *J. Phys. Chem. B* (1997) **101**, 4641.
[25] B. Markovsky, M. Levi and D. Aurbach, *Electrochim. Acta* **43** (1998) 2287.
[26] M. Tsionsky, G. Gun, V. Glezer and O. Lev, *Anal. Chem.*, **66** (1994) 1747.
[27] L. Rabinovich, J. Gun, O. Lev, D. Aurbach, B. Markovsky and M. D. Levi, *Adv. Mater.* **8** (1998) 577.
[28] W. Weppner and R. A. Huggins, *Ann. Rev. Mater. Sci.* **8** (1978) 269.
[29] C. J. Wen, B. A. Boukamp, R. A. Huggins and W. Weppner, *J. Electrochem. Soc.* **126** (1979) 2258.
[30] J. O'M Bockris and S. V. M. Khan, 'Surface Electrochemistry. A Molecular Level Approach', Plenum Press, New York (1993), p. 226.